Published in final edited form as:
Phys Med Biol. 2013 February 7; 58(3): 735–748. doi:10.1088/0031-9155/58/3/735.

Turbulent Water Coupling in Shock Wave Lithotripsy

Jaclyn Lautz, **Georgy Sankin**[a], and **Pei Zhong**
Department of Mechanical Engineering and Materials Science, Duke University, Durham, North Carolina 27708, USA

Abstract

Previous studies have demonstrated that stone comminution decreases with increased pulse repetition frequency as a result of bubble proliferation in the cavitation field of a shock wave lithotripter (Pishchalnikov *et al.*, 2011). If cavitation nuclei remain in the propagation path of successive lithotripter pulses, especially in the acoustic coupling cushion of the shock wave source, they will consume part of the incident wave energy, leading to reduced tensile pressure in the focal region and thus lower stone comminution efficiency. We introduce a method to remove cavitation nuclei from the coupling cushion between successive shock exposures using a jet of degassed water. As a result, pre-focal bubble nuclei lifetime quantified by B-mode ultrasound imaging was reduced from 7 s to 0.3 s by a jet with an exit velocity of 62 cm/s. Stone fragmentation (percent mass < 2 mm) after 250 shocks delivered at 1 Hz was enhanced from 22 ± 6% to 33 ± 5% ($p = 0.007$) in water without interposing tissue mimicking materials. Stone fragmentation after 500 shocks delivered at 2 Hz was increased from 18 ± 6% to 28 ± 8% ($p = 0.04$) with an interposing tissue phantom of 8 cm thick. These results demonstrate the critical influence of cavitation bubbles in the coupling cushion on stone comminution and suggest a potential strategy to improve the efficacy of contemporary shock wave lithotripters.

1. Introduction

Shock wave lithotripsy (SWL) is the front-line treatment for kidney stone disease, a painful medical condition that affects more than 10% of the population in the United States (Center-for-Disease-Control-and-Prevention, 2010). Traditionally, SWL treatment was performed by placing a patient in a large water tub (e.g., “wet” coupling in the first-generation Dornier HM3 lithotripter). In contrast, contemporary lithotripters utilize “dry” coupling, in which a water-filled cushion with a silicone membrane in contact with the patient’s skin is used to facilitate shock wave transmission into the patient (Neucks *et al.*, 2008). To the best of our knowledge, there is no consensus regarding the quality control or circulation conditions of the water inside the cushion of contemporary clinical shock wave lithotripters. Previous studies have shown that stone comminution is reduced as pulse repetition frequency (PRF) increases (Greenstein and Matzkin, 1999; Weir *et al.*, 2000; Paterson *et al.*, 2002; Madbouly *et al.*, 2005; Kato *et al.*, 2006)which may be caused in part by cavitation in the coupling medium (i.e., both water in the cushion and ultrasound gel between the cushion and patient’s body).

Cavitation in the coupling media can be initiated at nucleation sites (Apfel, 1984; Sankin and Teslenko, 2003), which are micro- and nano-meter sized bubbles or gas pockets stabilized on solid particles or surfaces, by the tensile phase of a lithotripter shock wave (LSW). Cavitation bubbles continue to expand after the shock wave has passed, gas diffuses into the expanding bubbles which grow several orders of magnitude in size (Coleman *et al.*,

[a]gns@duke.edu.

1987; Church, 1989), and eventually the static pressure in the fluid forces the bubbles to violently collapse. Upon non-spherical collapse and fragmentation these bubbles can generate a myriad of micron-sized "daughter bubbles" that can serve as nuclei for new cavitation events induced by subsequent LSWs (Huber *et al.*, 1999; Pishchalnikov *et al.*, 2011). Typically, the dissolution time of bubbles generated by an incident shock wave is much longer than the interpulse time of the lithotripter pulses (Sapozhnikov *et al.*, 2002). Therefore, strong cavitation in the coupling liquid (water) develops within several shocks (Yong *et al.*, 2011). Moreover, it has been observed that cavitation activity in SWL can be enhanced substantially at higher PRFs (Zeman *et al.*, 1990). This is because of the influence of buoyancy and acoustic radiation force on microbubbles and cavitation proliferation in a quasi-static fluid is negligible when the time between successive shocks is relatively short (for PRF ≥ 1 Hz).

More importantly, bubbles produced in the coupling cushion of a lithotripter will selectively transmit the leading compressive component of the LSW while truncating its trailing tensile component (Voronin *et al.*, 2003; Pishchalnikov *et al.*, 2005). Cavitation in the coupling fluid consumes part of the incident shock wave energy, especially the tensile component, and thus greatly reduces cavitation in the focal region surrounding the stone, which is known to be critical for producing fine fragments (Zhu *et al.*, 2002; Sapozhnikov *et al.*, 2007). Numerical calculations (Liebler *et al.*, 2006) suggest that the acoustic energy delivered to the focal region depends on the concentration of cavitation nuclei. Cavitation nuclei can be temporally deactivated by water degassing or by chemical additives. Chemical additives (acetic acid) were shown to reduce Harvey's cavitation nuclei by dissolving mineral particles (Eisenmenger and Pecha, 2003). Cavitation can also be minimized by a weak preceding shock wave that diminishes the number of cavitation sites of particles in the focal volume (Arora *et al.*, 2005). However, bubble proliferation is the dominant factor in determining cavitation activity after several shocks. If cavitation in the coupling cushion is related to the decreased stone comminution, then reducing the number or density of cavitation nuclei in the fluid along the LSW pathway between successive shocks will enable an increase in shock wave delivery rate without negatively affecting stone comminution.

In this work, we have developed a method to continuously convect the fluid in the coupling cushion of a lithotripter via a turbulent jet in order to minimize the accumulation of bubble nuclei along the LSW propagation path during SWL. Using this strategy, we have demonstrated that the tensile wave of the LSW at the lithotripter focus is better preserved even at high PRFs and more effective stone comminution can be produced. The implication of this method of cavitation control to studying tissue injury and improving the efficiency of SWL will be discussed.

2. Experimental Methods

2.1. Electromagnetic shock wave source and acoustic coupling

A schematic diagram of the experimental setup is shown in figure 1. An experimental electromagnetic shock wave source with an acoustic lens of 140 mm in focal length was used. The shock source, mounted in an acrylic tank tilted at an 8 degree angle, was controlled by a pulse generator (BNC Model 555) to deliver shock waves at a specific PRF ranging from 0.5 to 3 Hz. A peristaltic pump (Cole Palmer, 77200-60) that generates intermittent flow was connected to an open port at the center of the shock wave source to circulate degassed and filtered water into the tank. The pump-generated jet flow was used to flush and disperse water off the LSW propagation path at a specified flow rate Q. Throughout the experiments, the pump was used to generate either a puff flow (Nishi *et al.*, 2008) at Q = 6.5 cm^3/s, [Supplemental movie 1] or a turbulent jet [(Landau and Lifshitz,

1987) page 147] at Q = 15.9 and 35.7 cm^3/s [Supplemental movie 2]. The jet flow can be characterized by the Reynolds number:

$$Re=UD/\nu \quad (1)$$

where $U = 4Q/\pi D^2$ is the jet exit velocity, D = 8.6 mm is the nozzle diameter, and $v = 0.9\times10^{-6}$ m^2/s is the kinematic viscosity of water at 25°C. When the Reynolds number exceeds Re* = 1500, the jet flow becomes turbulent with an open angle of 22 degrees (Ungate *et al.*, 1975) confirmed by flow visualization. The corresponding flow rate Q* = 9 cm^3/s (U* = 15.5 cm/s) can be used to define the transition from puff flow to turbulent flow.

Two different experimental configurations were evaluated. In the first experiment [figure 1(a)], the water jet was released into a water tank representing "wet" coupling. In the second experiment [figure 1(b)], the jet flow was constrained by a cylindrical acrylic chamber ($\varnothing_{in}$ = 127 mm) with a 0.5 mm thick silicone rubber membrane (arrow "A") on top to mimic "dry" coupling. The jet flow initially propagates vertically followed by deflection downward and out of the chamber through the holes along its perimeter. In addition, a second chamber filled with butanediol (1,3-butanediol, Sigma Aldrich), a viscous liquid that has acoustic properties similar to soft tissue (Granz, 1994) was employed as a tissue phantom above the coupling chamber. Another silicone membrane was attached to this chamber (arrow "B") to separate it from the stone holder. The thickness "H" of the tissue phantom was varied from 50 mm to 80 mm based on the range of skin-to-stone distances observed in patients (Pareek *et al.*, 2005). The height h (= 140 mm – H) of the water coupling chamber was adjusted accordingly to maintain the same distance from the shock source aperture to the stone. Because of higher wave attenuation in butanediol than in water, the lithotripter output voltage setting was increased when the tissue phantom was employed in order to ensure that a peak positive pressure (p_+) of more than 30 MPa could be delivered to the stone.

2.2. Pressure measurements

The pressure waveforms at the focus of the shockwave source were measured using a fiber optic probe hydrophone (FOPH-500, RP Acoustics, Leutenbach, Germany), which has been shown to accurately measure the acoustic field with minimal cavitation induced artifacts (Smith *et al.*, 2012). In free field, 20 measurements were made at each PRF of 1, 2, or 3 Hz with or without the jet. Since after the initial 5 shocks cavitation activity along the LSW path became stable, the average pressure waveform was calculated from the 5^{th} to 20^{th} shocks. Attenuation in the tissue phantom was measured at 5 mm above the focus to avoid reflection of the FOPH laser from the silicone rubber membrane. The peak pressure dropped from 40 ± 1 MPa in free field to 34 ± 1 MPa with the 50 mm chamber and to 33 ± 1 MPa with the 80 mm chamber [figure 1(c, d)]. Furthermore, the tensile component of the LSW pulse was truncated by the tissue phantom compared to that in free field, which is in accordance with previous observations (Granz, 1994).

2.3. Cavitation assessment

Cavitation activity produced along the LSW propagation path was captured by shadowgraph imaging using a high-speed camera (Phantom v.7.3, Vision Research, Wayne, NJ) at a framing rate of 18,000 - 20,000 frames/s and an exposure time of 10 μs. The acquired images were post-processed off-line in Matlab (R2010b, MathWorks, Natick, MA) and the cavitation index (Sankin, 2002; Sankin, 2006) was quantified as the area shadowed by bubbles in a specified region of interest (ROI). Two 40 mm wide ROIs were selected: I) below the tissue phantom in the water coupling region (−83 mm < z < −53 mm) and II) above the tissue phantom near the focus (−3 mm < z < +27 mm) with z = 0 mm denoting the lithotripter focus.

In addition, cavitation nuclei distribution in the ROI was visualized by B-mode ultrasound using a SonoSite 180Plus with a 15 mm array transducer (C15/4-2 MHz, SonoSite Inc., Bothell, WA), as shown previously by others (Coleman *et al.*, 1995; Tu *et al.*, 2007). Based on the Minnaert approximation (Minnaert, 1933), the resonant radius a_0 of microbubbles in water that are acoustically detectable at $f_0 = 2$ MHz is:

$$a_0 = f_0 \cdot 3.26\ \mathrm{m/s} = 1.6\mu\mathrm{m} \quad (2)$$

The B-mode ultrasound transducer was mounted on the side of the water tank [figure 1(a)] and positioned to image microbubbles above a_0 and below the optical resolution of the high-speed camera (250 μm / pixel) at a 29.97 frames per second frame rate. The ultrasound images were recorded to a computer for off-line processing using a video converter (VideoMate U900, Compro Technology, Inc).

2.4. Stone treatment and statistical analysis

A flat-base stone holder made from a Teflon® tube ($\varnothing_{in}$ = 14 mm, $\varnothing_{out}$ = 17 mm) was sealed at one end with a 0.78 mm thick silicone rubber membrane [figure 1(e)]. Cylindrical stone phantoms (7 mm × 7 mm) made of Bego® powder (BEGO USA, Smithfield, RI) and water at a 5:2 (Bego powder:water) mixing ratio (Esch *et al.*, 2010) were pre-soaked in water for 2 hours before experiments [figure 1(e)]. Stones were treated with 250 shocks at varying PRF rates (1, 2, and 3 Hz) in free field. In the tissue phantom setup, stones were treated with 250 shocks (H = 50 mm, $p_+ = 35 \pm 1$ MPa) and with 500 shocks (H = 80 mm, $p_+ = 37 \pm 1$ MPa) both at 2 Hz PRF. The experiments were repeated with and without the turbulent jet ($n = 5 \sim 6$). Afterwards, stone fragments were dried in an oven at 40°C for 24 hours and then passed sequentially through a series of sieves of 2 and 2.8 mm mesh sizes and weighed. Comminution efficiency was determined by the percent mass of fragments less than 2 mm unless otherwise specified. The two-tailed student t-test was used to calculate p-values and statistical significance was characterized by $p < 0.05$ corresponding to a 95% confidence interval.

3. Results

3.1. Cavitation in free field

Figures 2(a) and 3(a) show representative high-speed images of cavitation bubble clusters in free field during stone comminution experiments at a PRF = 3 Hz without and with the turbulent jet (Q = 35.7 cm^3/s), respectively. The expansion time of the bubble cluster in both cases is about 200 μs. In contrast, the collapse time of the bubble cluster is shortened significantly from 550 μs without the jet to 400 μs with the jet. In addition, the density of the bubble cluster appears to be reduced by the jet flow. Figure 2(b) and 3(b) show residual microbubble distribution formed along the LSW propagation path during four consecutive shocks without and with the jet, respectively. In both cases microbubbles are concentrated along the lithotripter axis. In the absence of the jet [figure 2(b)], B-mode ultrasound images recorded during the treatment (i.e., around the 200^{th} shock) reveal a larger microbubble cluster and longer nuclei lifetime than with the jet [figure 3(b)]. These microbubbles provide cavitation nuclei for the generation of a new bubble cluster by an ensuing shock wave. The lifetime of the microbubbles was quantified from the echogenecity in B-mode images following the last (i.e., 250^{th}) shock. Without the jet, the echogenicity lasted about 7 seconds [Supplemental movie 3], indicating that the bubble nuclei persisted for a period much longer than the inter-pulse time between subsequent shocks (i.e., 1 s at 1 Hz PRF). In comparison, with the jet [figure 3(b)], the echogenicity disappeared within 0.3 s, which is shorter than the inter-pulse time (i.e., 0.33 s at 3 Hz PRF).

3.2. Acoustic rectification

To access the effects of cavitation along the propagation path on the lithotripter field, pressure waveforms were measured at the geometric focus of the shock wave source at different PRFs and compared with a reference waveform taken at a PRF < 0.05 Hz. In general the positive peak pressure (p_+) of the LSW is neither sensitive to the turbulence nor to the cavitation and measured 42 ± 2 MPa (mean ± std). In contrast the tensile peak pressure (p_-) and tensile pulse duration (t_-) decrease with PRF. The rectification effect (reduction and shortening of the tensile component) is maximized without the jet [figure 4(a, c, e)], under which condition p_- values are reduced from −8.6 MPa (single shock) to −3.9, −2.6, and −2.5 MPa at 1, 2 and 3 Hz of PRF, respectively. In addition, t_- is shortened from 4.3 μs (single shock) to 3 μs at 1 Hz and 2.6 μs at 2 and 3 Hz. The jet was found to have a strong effect in preserving the tensile component of the LSW [figure 4(b, d, f)]. For example, at 1 Hz PRF, p_- of −8.0 MPa and t_- of 4.3 μs were measured, approaching the corresponding values (p_- = −8.6 MPa and t_- = 4.3 μs) from a single shock. This trend continues at PRFs of 2 and 3 Hz with corresponding values of p_- reduced to −6.2 and −5.6 MPa, while t_- shortened to 3.6 and 3 μs, respectively. Altogether, these results suggest that using a jet can regulate acoustic rectification of the tensile component.

3.3. Cavitation with the tissue phantom

The turbulent jet was found to significantly affect the cavitation activities both in the water coupling chamber and in the focal region. As shown in figure 5(a, c), the jet dramatically reduces the maximum cavitation index (C_{max}) in the water coupling chamber from 3.4 cm^2 (without the jet) to 1.2 cm^2 (with the jet). This reduction of cavitation in the water coupling chamber led to a corresponding enhancement of cavitation activity in the focal area from 0.9 cm^2 (without the jet) to 2.2 cm^2 (with the jet). As shown in figure 5(b) and figure 5(d), the collapse time of the bubble cluster in the focal region is significantly longer with (~385 μs) than without (~275 μs) the jet while in contrast, bubble collapse time in the water coupling chamber is shortened from ~495 μs to ~275 μs by the use of the jet. This inverse correlation between the bubble activities in the focal region and those in the water coupling chamber demonstrates the feasibility of using a turbulent jet to control cavitation in the focal region.

The maximum cavitation index C_{max} in the coupling chamber was averaged (n = 15 shocks) for different PRFs and pumping flow rates (Q) [Figure 6(a)]. At PRF = 0.05 Hz, C_{max} does not depend on Q and is equal to 0.17 ± 0.02 cm^2 (n = 4, data not shown). As PRF increases, C_{max} generally increases regardless of Q. Particularly without the jet C_{max} increases rapidly and exceeds by three fold the corresponding value of 0.6 cm^2 with the jet (at 1 Hz PRF). At PRF = 3 Hz, C_{max} further increases to 3.7 cm^2 and remains above 3 cm^2, 1.9 cm^2, and 1.6 cm^2 at flow rates of 6.5 cm^3/s, 15.9 cm^3/s, and 35.7 cm^3/s, respectively. It is worth noting that the data from the lowest flow rate (6.5 cm^3/s) at 2 and 3 Hz converges with results without the jet. The difference in maximum cavitation index ΔC_{max} with and without the jet at different flow rates is shown in figure 6(b). The curve corresponding the lowest flow rate (Q = 6.5 cm^3/s) reaches a distinct peak at 1 Hz. The peak is shifted toward higher PRF values with pumping rate indicating the critical role of the jet velocity.

3.4. Stone comminution

Stone comminution was obtained at the fastest flow rate, Q = 35.7 cm^3/s since it minimizes cavitation activity in the coupling chamber. As shown in figure 7, stone comminution after 250 shocks in free field is more effective with than without the jet, although in general, fragmentation efficiency reduces as PRF increases in both cases. At 1 Hz PRF, stone fragmentation is 22 ± 6% without the jet compared to 33 ± 5% with the jet (p = 0.007). Similarly, at 2 Hz PRF stone fragmentation is 19 ± 5% without the jet, which is significantly lower than 26 ± 6% with the jet (p = 0.04). Stone fragmentation is about 23% at 3 Hz both

without and with the jet. Similar trends are observed for stone fragmentation characterized by percent mass < 2.8 mm [figure 7, solid symbols].

Although stone fragmentation is reduced with an interposing tissue phantom [figure 8(a)] compared to the corresponding value in free field [figure 7], fragmentation efficiency can be improved by using the jet. After 250 shocks, stone fragmentation in the 90-mm coupling chamber (with 50-mm thick tissue phantom) increased from 14 ± 3% without the jet to 22 ± 7% with the jet ($p = 0.03$). Similarly, after 500 shocks, stone fragmentation in the 60-mm coupling chamber (with 80-mm thick tissue phantom) increased from 18 ± 6% without the jet to 28 ± 8% with the jet ($p = 0.04$) [figure 8(b)]. Altogether, stone fragmentation results both in free field and with tissue phantoms have demonstrated the effectiveness of the jet in enhancing stone fragmentation in the focal region by minimizing pre-focal cavitation.

4. Discussion

Cavitation in the coupling liquid (water) has a significant impact on the pressure waveform, acoustic energy and stone comminution efficiency produced in the lithotripter focal region. Even with careful water preparation (degassing and filtering), abundant pre-focal cavitation can be developed following a few lithotripter pulses. Although only a few bubble nuclei may exist initially in the coupling cushion prior to SWL, an avalanche of bubbles will be generated during the subsequent shock wave exposures. As a result, significant amounts of residual cavitation nuclei persist along the LSW propagation path between successive shocks, as revealed by B-mode ultrasound imaging [figure 2(b)]. Consequently, shock wave transmission towards the focal region will be significantly reduced, manifested by the truncation of the trailing tensile component of the LSW [figure 4], which has also been shown in previous studies (Pishchalnikov *et al.*, 2005). For this reason, the treatment time in clinical SWL is practically limited by the pulse delivery rate (i.e. 60 - 120 shocks per minute) regardless of the lithotripter type (Rassweiler *et al.*, 2011). However, by reducing the cavitation activity in the coupling cushion, more effective cavitation can be produced in the focal region, leading to improved stone comminution. The feasibility of this beneficial strategy has been demonstrated in this study, which provides an alternative to the conventional approach to improve stone comminution via increasing the output energy of the lithotripter that will concomitantly elevate the risk of tissue injury.

We have developed a turbulent jet technique in this study to disperse residual cavitation nuclei along the LSW propagation pathway in the coupling cushion of the shock wave generator. Furthermore, we have demonstrated that by using a jet with an exit velocity of 62 cm/s the lifetime of bubble nuclei in the coupling water can be reduced from ~ 7 s (without the jet) to ~ 0.3 s, which is shorter than the interpulse time between successive pulses under the highest PRF of 2 Hz used clinically (Rassweiler *et al.*, 2011). This substantial reduction in cavitation activity in the pre-focal region helps to preserve the tensile pressure (p_-) of the LSW delivered to the focal region [figure 4], and thus enhance the cavitation activity in the focal region and consequently stone comminution [figure 7 and figure 8]. These findings are supported by previous studies on the effect of cavitation activity in the LSW propagation path on resultant pressure waveform at the lithotripter focus, obtained both experimentally (Teslenko *et al.*, 1999; Pishchalnikov *et al.*, 2005) and through numerical model calculations (Liebler *et al.*, 2006; Krimmel *et al.*, 2010). The growth of cavitation nuclei in the pre-focal region consumes progressively the acoustic energy associated with the tensile component of the incident lithotripter pulses as they propagate towards the stone. If sufficient cavitation bubbles are formed along the pathway during SWL, most of the energy associated with the tensile pressure of the LSW will be depleted, leading to minimal cavitation activity produced around the target stone, and thus significantly decreased stone comminution (Zhu *et al.*, 2002). Based on this understanding, if cavitation activity in the pre-focal region can be substantially suppressed, more tensile pressure of the LSW will be preserved during

propagation to reach the stone for better comminution. Our results have demonstrated that the jet can the effectively reduce the density of cavitation nuclei in the coupling cushion even at 2 Hz PRF, leading to better preserved tensile pressure and pulse profile of the LSW delivered to the focus of the lithotripter.

We have further investigated the correlation between cavitation induced in the coupling cushion and the bubble activities produced in the focal region using tissue mimicking phantoms. In general, we have observed that the effectiveness of acoustic coupling depends on the cushion thickness (h), the pulse repetition frequency (PRF), and the jet exit velocity (U). At a low PRF (< 0.5 Hz), the flow rate is insignificant because cavitation nuclei can be dissolved and/or removed by a convective flow induced by acoustic radiation force produced by the incident LSW. However, as PRF increases, a higher flow rate is required to reduce the concentration of residual bubble nuclei between successive shocks. The effectiveness of the turbulent jet in removing bubble nuclei can be described by a dimensionless number $\Lambda = PRF\ h/U$ [Table 1], which defines the fluid exchange rate in the constrained water volume between lithotripter pulses. Indeed, a correlation between Λ and stone comminution supports the idea that circulating the larger liquid volume in the cushion optimizes the coupling conditions in the focal area. Therefore, we approximate that a Λ value less than or equal to 1 (shaded gray in Table 1) corresponds to experimental conditions that define effective flushing. As Λ becomes greater than 1, stone comminution becomes less successful as the cavitation nuclei linger between shocks.

Our findings show that suppressing bubble proliferation in the coupling cushion can improve the effectiveness and efficiency of SWL by enhancing the tensile component of the LSW delivered to the focal region. Previous studies have demonstrated that step-wise “ramping up” of the output energy of the lithotripter is an effective treatment strategy to improve stone comminution (Zhou *et al.*, 2004; Demirci *et al.*, 2007; Lambert *et al.*, 2010). Furthermore, future lithotripter designs may include a longer focal distance to accommodate the increasing rate of overweight patients in clinic. However, for slim patients, the cushion geometry would have to be more inflated than an obese patient to account for the longer focal distance. All these scenarios suggest the need to control acoustic properties of the water inside the cushion of future clinical shock wave lithotripters. Using this new water coupling technique, the energy associated with the tensile component of the LSWs can be adjusted, introducing a method for controlling cavitation in SWL. Cavitation in the coupling fluid may also depend on overpressure and water temperature, which warrant further studies.

5. Conclusion

In this study we have investigated the effects of a flushing jet of degassed water along the lithotripter propagation pathway on cavitation activity in the lithotripter focus and in the coupling cushion. By varying PRF, cushion thickness, and the pumping flow rate it was demonstrated that if residual nuclei were removed between successive pulses, the tensile component of the LSWs delivered to the lithotripter focus could be better preserved with enhanced stone fragmentation *in vitro.* Future studies are warranted to assess the effects of this novel coupling technique on stone comminution and tissue injury *in vivo*. We hypothesize that the peak pressure and acoustic pulse energy levels can be lowered at a faster PRF (e.g., 2 Hz) that possess minimal risk for tissue injury while shortening treatment time as a result of improved acoustic transmission.

Supplementary Material

Refer to Web version on PubMed Central for supplementary material.

Acknowledgments

This work was supported by the NIH through grants R37-DK052985 and S10-RR16802 and by the NSF Graduate Research Fellowship Program (JL). We thank Pratt Machine Shop, especially Mr. John Goodfellow, for technical assistance and Siemens for providing the electromagnetic shock wave sources used in the experiments.

References

Apfel RE. Acoustic cavitation inception. Ultrasonics. 1984; 22:167–73.

Arora M, Junge L, Ohl CD. Cavitation cluster dynamics in shock-wave lithotripsy: part 1. Free field *Ultrasound in Medicine and Biology*. 2005; 31:827–39.

Center-for-Disease-Control-and-Prevention. National Chronic Kidney Disease Fact Sheet: general information and national estimates on chronic kidney disease in the United States. U.S. Department of Health and Human Services; 2010.

Church CC. A theoretical study of cavitation generated by an extracorporeal shock wave lithotripter. The Journal of the Acoustical Society of America. 1989; 86:215–27. [PubMed: 2754108]

Coleman AJ, Kodama T, Choi MJ, Adams T, Saunders JE. The cavitation threshold of human tissue exposed to 0.2-MHz pulsed ultrasound: Preliminary measurements based on a study of clinical lithotripsy. Ultrasound in Medicine & Biology. 1995; 21:405–17. [PubMed: 7645132]

Coleman AJ, Saunders JE, Preston RC, Bacon DR. Pressure waveforms generated by a Dornier extra-corporeal shock-wave lithotripter. Ultrasound in medicine & biology. 1987; 13:651–7. [PubMed: 3686729]

Demirci D, Sofikerim M, Yalcin E, Ekmekcioglu O, Gulmez I, Karacagil M. Comparison of conventional and step-wise shockwave lithotripsy in management of urinary calculi. J Endourol. 2007; 21:1407–10. [PubMed: 18044996]

Eisenmenger, W.; Pecha, R. Eine neue Art von Kavitationskeimen. Fortschritte der Akustik - DAGA 03′; Aachen, Deutschland. 2003. p. 842-3.

Esch E, Simmons W, Sankin G, Cocks H, Preminger G, Zhong P. A simple method for fabricating artificial kidney stones of different physical properties. Urol. Res. 2010; 38:315–9. [PubMed: 20652562]

Granz B. Measurement of Shock Wave Properties after the Passage through a Tissue Mimicking Material. Ultrason. 1994:1847–51.

Greenstein A, Matzkin H. Does the rate of extracorporeal shock wave delivery affect stone fragmentation? Urology. 1999; 54:430–2. [PubMed: 10475348]

Huber P, Debus J, Jochle K, Simiantonakis I, Jenne J, Rastert R, Spoo J, Lorenz WJ, Wannenmacher M. Control of cavitation activity by different shockwave pulsing regimes. Physics in medicine and biology. 1999; 44:1427–37. [PubMed: 10498515]

Kato Y, Yamaguchi S, Hori J, Okuyama M, Kakizaki H. Improvement of stone comminution by slow delivery rate of shock waves in extracorporeal lithotripsy. Int J Urol. 2006; 13:1461–5. [PubMed: 17118017]

Krimmel J, Colonius T, Tanguay M. Simulation of the effects of cavitation and anatomy in the shock path of model lithotripters. Urol. Res. 2010; 38:505–18. [PubMed: 21063697]

Lambert E, Walsh R, Moreno MW, Gupta M. Effect of escalating versus fixed voltage treatment on stone comminution and renal injury during extracorporeal shock wave lithotripsy: a prospective randomized trial. The Journal of urology. 2010; 183:580–4. [PubMed: 20018316]

Landau, LD.; Lifshitz, EM. Fluid Mechanics. Butterworth-Heinemann; 1987.

Liebler M, Dreyer T, Riedlinger RE. Modeling of interaction between therapeutic ultrasound propagation and cavitation bubbles. Ultrasonics. 2006; 44:E319–E24. [PubMed: 16908041]

Madbouly K, El-Tiraifi AM, Seida M, El-Faqih SR, Atassi R, Talic RF. Slow versus fast shock wave lithotripsy rate for urolithiasis: a prospective randomized study. The Journal of urology. 2005; 173:127–30. [PubMed: 15592053]

Minnaert M. On musical air bubbles and the sounds of running water. Philos Mag. 1933; 16:235–48.

Neucks JS, Pishchalnikov YA, Zancanaro AJ, VonDerHaar JN, Williams JC, McAteer JA. Improved acoustic coupling for shock wave lithotripsy. Urol. Res. 2008; 36:61–6. [PubMed: 18172634]

Nishi M, Unsal B, Durst F, Biswas G. Laminar-to-turbulent transition of pipe flows through puffs and slugs. J Fluid Mech. 2008; 614:425–46.

Pareek G, Hedican SP, Lee FT Jr, Nakada SY. Shock wave lithotripsy success determined by skin-to-stone distance on computed tomography. Urology. 2005; 66:941–4. [PubMed: 16286099]

Paterson RF, Lifshitz DA, Lingeman JE, Evan AP, Connors BA, Fineberg NS, Williams JC Jr. McAteer JA. Stone fragmentation during shock wave lithotripsy is improved by slowing the shock wave rate: studies with a new animal model. The Journal of urology. 2002; 168:2211–5. [PubMed: 12394761]

Pishchalnikov YA, Sapozhnikov OA, Bailey MR, Pishchalnikova IV, Williams JC, McAteer JA. Cavitation selectively reduces the negative-pressure phase of lithotripter shock pulses. Acoustics research letters online : ARLO. 2005; 6:280–6. [PubMed: 19756170]

Pishchalnikov YA, Williams JC, McAteer JA. Bubble proliferation in the cavitation field of a shock wave lithotripter. The Journal of the Acoustical Society of America. 2011; 130:EL87–93. [PubMed: 21877776]

Rassweiler JJ, Knoll T, Kohrmann KU, McAteer JA, Lingeman JE, Cleveland RO, Bailey MR, Chaussy C. Shock wave technology and application: an update. Eur Urol. 2011; 59:784–96. [PubMed: 21354696]

Sankin, G. Dynamics and luminescence of bubble cluster in a focused bipolar acoustic wave (PhD Thesis). Russian Academy of Sciences; Novosibirsk: 2002. p. 121

Sankin G. Cavitation under spherical focusing of acoustic pulses. Acoustical Physics. 2006; 52:93–103.

Sankin G, Teslenko V. Two-threshold cavitation regime. Doklady Physics. 2003; 48:665–8.

Sapozhnikov OA, Khokhlova VA, Bailey MR, Williams JC Jr. McAteer JA, Cleveland RO, Crum LA. Effect of overpressure and pulse repetition frequency on cavitation in shock wave lithotripsy. The Journal of the Acoustical Society of America. 2002; 112:1183–95. [PubMed: 12243163]

Sapozhnikov OA, Maxwell AD, MacConaghy B, Bailey MR. A mechanistic analysis of stone fracture in lithotripsy. The Journal of the Acoustical Society of America. 2007; 121:1190–202. [PubMed: 17348540]

Smith N, Sankin GN, Simmons WN, Nanke R, Fehre J, Zhong P. A comparison of light spot hydrophone and fiber optic probe hydrophone for lithotripter field characterization. The Review of scientific instruments. 2012; 83:014301. [PubMed: 22299970]

Teslenko VS, Sankin GN, Drozhzhin AP. Luminescence in water and glycerin in the field of spherically focused and plane shock-acoustic waves. Combust. Explos. 1999; 35:717–20.

Tu J, Matula TJ, Bailey MR, Crum LA. Evaluation of a shock wave induced cavitation activity both in vitro and in vivo. Physics in medicine and biology. 2007; 52:5933–44. [PubMed: 17881810]

Ungate, CD.; Harleman, DRF.; Jirka, GH. Stability and mixing of submerged turbulent jets at low reynolds numbers. Energy Laboratory, Massachusetts Institute of Technology; 1975.

Voronin D, Sankin G, Teslenko V, Mettin R, Lauterborn W. Secondary Acoustic Waves in a Polydisperse Bubbly Medium. Journal of Applied Mechanics and Technical Physics. 2003; 44:9.

Weir MJ, Tariq N, Honey RJ. Shockwave frequency affects fragmentation in a kidney stone model. J Endourol. 2000; 14:547–50. [PubMed: 11030533]

Yong DZ, Lipkin ME, Simmons WN, Sankin G, Albala DM, Zhong P, Preminger GM. Optimization of Treatment Strategy Used During Shockwave Lithotripsy to Maximize Stone Fragmentation Efficiency. J. Endourol. 2011; 25:1507–11. [PubMed: 21834658]

Zeman RK, Davros WJ, Garra BS, Horii SC. Cavitation effects during lithotripsy. Part I. Results of in vitro experiments. Radiology. 1990; 177:157–61. [PubMed: 2204961]

Zhou Y, Cocks FH, Preminger GM, Zhong P. The effect of treatment strategy on stone comminution efficiency in shock wave lithotripsy. The Journal of urology. 2004; 172:349–54. [PubMed: 15201809]

Zhu S, Cocks FH, Preminger GM, Zhong P. The role of stress waves and cavitation in stone comminution in shock wave lithotripsy. Ultrasound in medicine & biology. 2002; 28:661–71. [PubMed: 12079703]

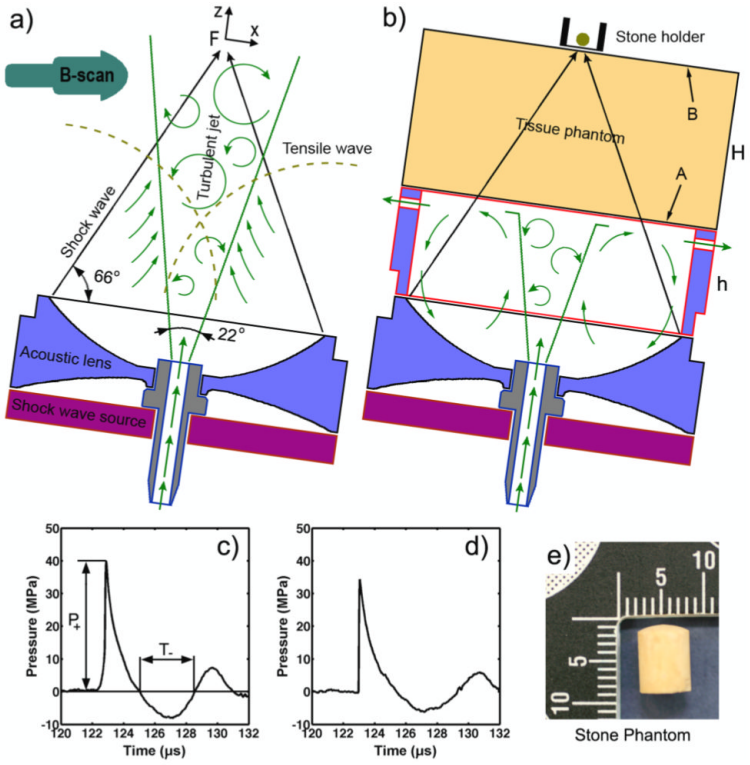

Figure 1.

Schematic diagram of the experimental setup showing an electromagnetic shock wave source with an acoustic lens (focal distance f = 140 mm) in free field (a) and with the cushion (b). The cushion setup also included a layer of viscous liquid of thickness “H” between the shock wave source and the stone holder to serve as a tissue phantom. The peak pressure (p_+) and the tensile duration (t_-) were measured at the focus “F” in free field (c) and with the tissue phantom (d; H = 80 mm). A cylindrical stone phantom of 7×7 mm in diameter and height (e) was placed in a stone holder at the lithotripter focus. Jet flow was introduced to the setup by pumping degassed water through the central port in the shock wave source to disperse residual cavitation nuclei along the shock wave path.

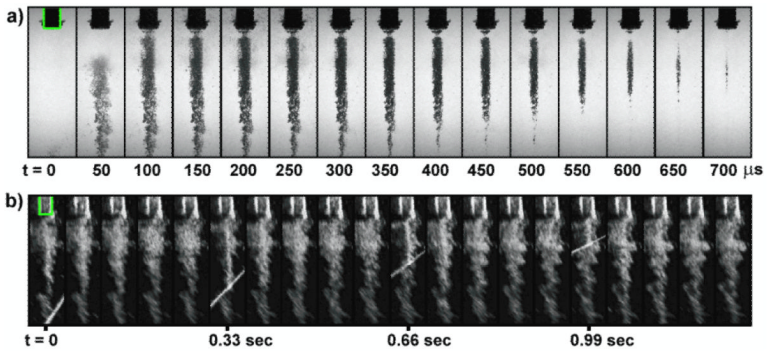

Figure 2.

Representative image sequences of cavitation during stone comminution experiments in free field (PRF = 3 Hz) without the jet. The shadowgraph high-speed image series (a) were captured after the 20th shocks using a 10 μs exposure time. The B-mode ultrasound images (b) were recorded during the experiment (around the 200th shock) to observe nuclei persistence during subsequent shockwave exposures. Bright rays seen on several B-mode image frames correspond to the interference produced by the release of lithotripter shock wave. The lifetime of detectable bubble nuclei is ~7 seconds. The stone holder $\varnothing_{out}$ = 17 mm) is highlighted in the first frame.

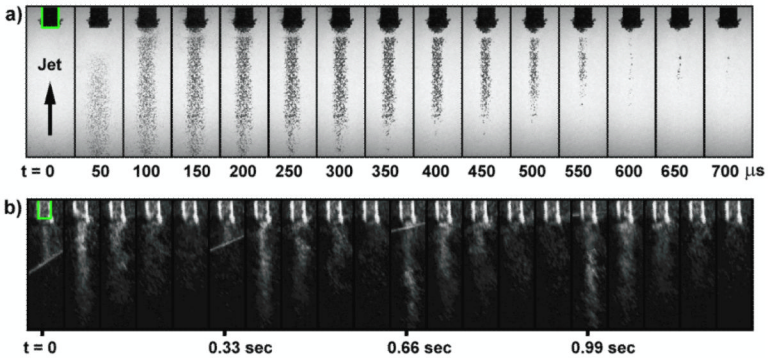

Figure 3.

Representative image sequences of cavitation during stone comminution experiments in free field (PRF = 3 Hz) with the jet. The shadowgraph high-speed image series (a) were captured after the 20th shocks using a 10 μs exposure time. The B-mode ultrasound images (b) were recorded during the experiment (around the 200th shock) to observe the reduction in nuclei lifetime along the LSW pathway. Bright rays seen on several B-mode image frames correspond to the interference produced by the release of lithotripter shock wave. The lifetime of detectable bubble nuclei is less than 0.3 seconds. The stone holder $\varnothing_{out}$ = 17 mm) is highlighted in the first frame.

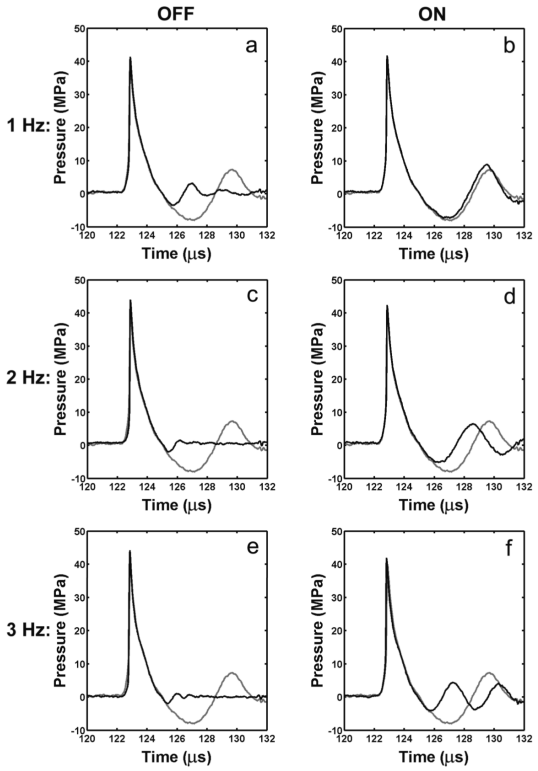

Figure 4.

Average pressure waveforms (n = 5, dark curves) at different PRFs of 1 (a, b), 2 (c, d), 3 Hz (e, f) without (a, c, e) and with (b, d, f) the jet in comparison with the average pressure waveform of single shock waves produced at a low PRF of < 0.05 Hz (n = 5) (light curve).

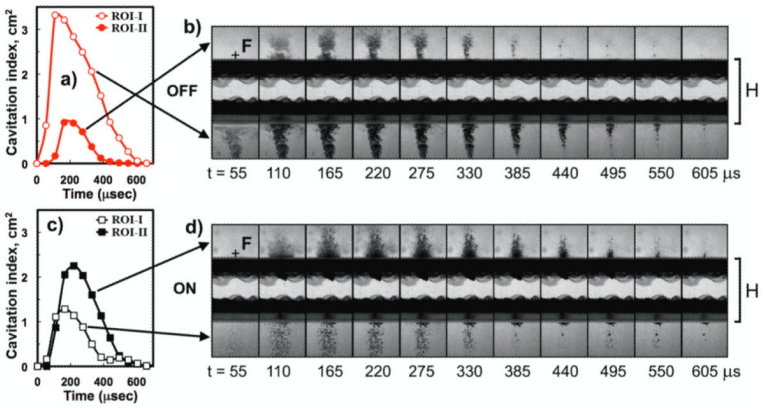

Figure 5.

Cavitation index as a function of time in two regions of interest separated by the tissue mimicking material (i.e., focal ROI-II and pre-focal ROI-I, n=15) produced at a PRF of 2 Hz without (a, b) and with (c, d) the jet. Pre-focally, cavitation index is higher without (open circles) than with (open squares) the jet. In the focus, cavitation index is greater with (solid squares) than without (solid circles) the jet. Representative high-speed shadowgraph images were captured using a framing rate of ~18,000 frames/second with an exposure time of 10 μs (H = 50 mm).

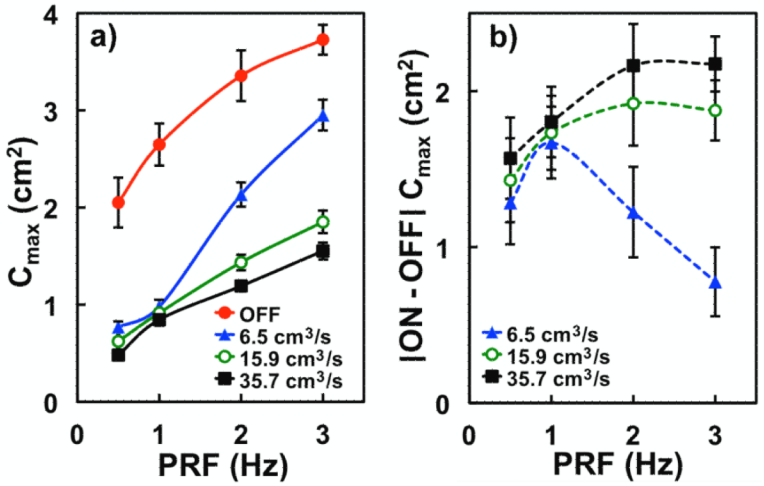

Figure 6.

(a) Maximum cavitation index in the cushion (ROI-I) at different PRFs, without (filled circles) and with the jet at three different pumping flow rates: Q = 6.5 cm^3/s (triangles), 15.9 cm^3/s (open circles) and 35.7 cm^3/s (squares). (b) Difference between maximum cavitation index (ROI-I) with the jet and without the jet at different PRFs. Error bars represent standard deviation (n = 25).

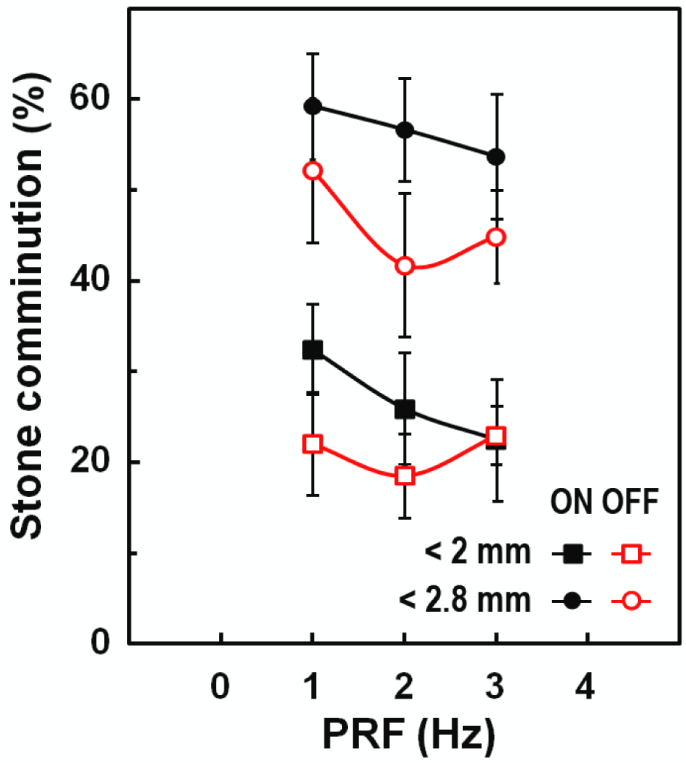

Figure 7.

Stone comminution in free field (p_+ = 41 MPa, Q = 35.7 cm^3/s) after 250 shocks delivered at different PRFs. The average values from 6 experiments under each condition are displayed for percent of fragments < 2.8 mm with (solid circles) and without (open circles) the jet, and also for percent of fragments < 2.0 mm with (solid squares) and without (open squares) the jet.

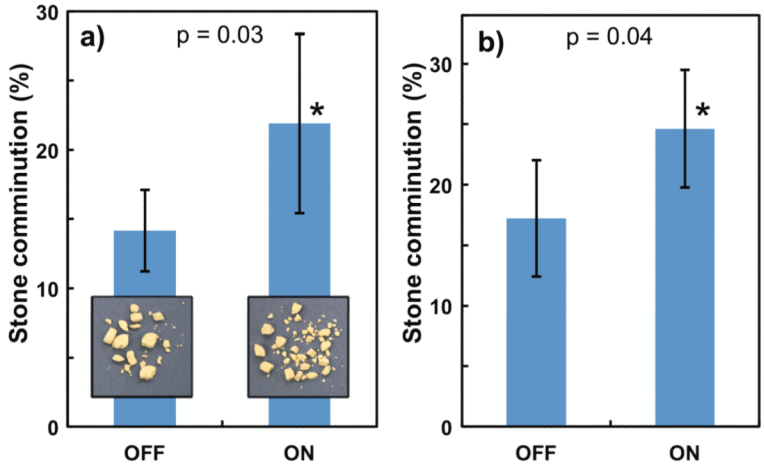

Figure 8.

Effect of the jet on stone comminution (determined by the percent of fragments < 2.0 mm) after 250 shocks (a; H = 50 mm, p_+ = 37 MPa) and 500 shocks (b; H = 80 mm, p_+ = 35 MPa). Both experiments were repeated 6 times using a PRF of 2 Hz and Q = 35.7 cm^3/s.

Table 1

Dimensionless number $\Lambda = PRF\ h/U$ for different flow rates and treatment regimes as an indicator of the effectiveness ($\Lambda \leq 1$, shaded gray) of the jet flow in the water coupling chamber (h = 90 mm).

Q (cm^3/s)	U (cm/s)	Re	Λ			
			0.5	1 Hz	2 Hz	3 Hz
6.5	11	1050	0.51	1.0	2.0	3.1
15.9	27	2580	0.21	0.42	0.85	1.3
35.7	62	5920	0.09	0.19	0.37	0.56